Ensuring Radio Frequency Compatibility (RFC) on-Board a Satellite by Early Analysis and Efficient Methods for Field Prediction

Jens Timmermann

Electrical Systems (TSPET32)
Airbus DS GmbH
Friedrichshafen, Germany
email: Jens.J.Timmermann
@airbus.com

Christian Imhof

Electrical Systems (TSPET32)
Airbus DS GmbH
Friedrichshafen, Germany
email: Christian.Imhof
@airbus.com

Dieter Lebherz

Electrical Systems (TSPET32)
Airbus DS GmbH
Friedrichshafen, Germany
email: Dieter.Lebherz
@airbus.com

Jörg Lange

Electrical Systems (TSPET32)
Airbus DS GmbH
Friedrichshafen, Germany
email: Joerg.Lange
@airbus.com

Abstract—**Transmitters (=Tx) on-board a satellite generate an electromagnetic environment with potential impact on victim receivers (=Rx, e.g., instruments) placed nearby. Ensuring Radio Frequency Compatibility (RFC) on-board a satellite is hence an important point to be considered during satellite design and requires an optimized satellite configuration. This contribution concentrates on RFC issues in practical satellite design by considering the future MetOp-SG meteorological satellites: First, an overview is given summarizing the various transmitters and instrument receivers on-board the satellites. Then, the fundamentals of RFC analysis are presented showing the method how to compute the coupling factor between a Tx and a victim Rx. To improve the decoupling, MetOp-SG satellites are housing dedicated baffles between Tx and Rx antennas. Therefore, the contribution finally studies in detail the signal attenuation caused by a baffle by comparing two methods: field simulation and an extended knife-edge diffraction theory. By combining both methods, the overall engineering and computation effort to optimize the baffle design is minimized.**

Keywords- MetOp-SG; Radio Frequency Compatibility; coupling factor; knife-edge diffraction; baffle attenuation.

I. INTRODUCTION

Earth observation satellites typically house a variety of transmitters and very sensitive instruments receivers. Hereby, the signal is transmitted / received via dedicated antennas. Instruments may, e.g., sense the Earth atmosphere while the collected data is transmitted towards Ground by the on-board Tx antennas. It has to be ensured that the instrument receivers work properly in the electromagnetic environment generated by on-board Tx antennas. This means that the remaining signal at a victim receiver has to be below a specified value. As the dimension of a satellite is in the order of only a few meters, the distance between Tx and Rx antennas is quite small which makes it challenging to achieve Radio Frequency Compatibility (RFC) on-board a satellite.

Therefore, the configuration of a satellite has to be optimized w.r.t. RFC, which means that the positions and the orientations of Tx and Rx antennas play a significant role. Even in an early project phase, this aspect has to be considered to minimize the need for configuration changes in a later project phase. The approach is hence to define a preliminary configuration and to run an RFC analysis which investigates the coupling between critical Tx and Rx combinations. In an early project phase, the unintended signal at a victim receiver shall be well below (typically 20 dB) the maximum acceptable value, whereas the difference is called RFC margin. On the other side, a satellite configuration will not only be optimized w.r.t. RFC. Other aspects (such as center of mass, minimization of harness length etc.) have to be taken into account and will lead to some configuration changes. In the end, a compromise will be required ensuring positive margins in all considered disciplines.

As the optimization exercise is typically not finished in an early project phase, the approach is to run an RFC analysis based on a preliminary satellite configuration and to aim for high margins. After the global optimization exercise, the remaining RFC margins may be lower, typically above 6 dB and thus still fulfilling the needs.

This contribution is an extended version of [1] and considers RFC aspects for the future MetOp-SG satellites:

The European MetOp meteorological satellites currently in orbit will be replaced after 2020 by follow-on satellites with advanced instrumentation. MetOp-SG will ensure observations until approximately 2040 [2]. After successful finalization of ESA Phase A/B1 study by Airbus Defence and Space, the company has been nominated by EUMETSAT / ESA as prime contractor for the provision of the space segment of MetOp-SG. For this purpose, two satellites (Satellite A and Satellite B) with different scientific instruments are currently under development. Each satellite houses a variety of transmitters and instrument receivers being sensitive in the RF frequency range. Hence, ensuring RFC on-board the satellite is a major challenge.

Section II of this contribution gives an overview of the different transmitters and receivers on-board the MetOp-SG satellites. To improve the decoupling between critical Tx / Rx combinations, the satellite design encompasses baffles that shade the Line of Sight (LoS) between these critical combinations.

Section III deals with the fundamentals of RFC analysis by summarizing the computations to derive the coupling factor between a Tx and victim Rx antenna. This section also discusses possibilities to ensure sufficient decoupling.

The remaining sections deal in more detail with the influence of a baffle on the received field strength: Hereby, Section IV presents two general approaches (E-field simulation and a simplified method based on knife-edge diffraction) to determine the baffle attenuation. To improve the predicted field strength, Section V shows an expansion of knife-edge diffraction theory by inclusion of an angle-dependent antenna gain. Finally, this section compares the obtained results for the two approaches. It is shown that the simplified theory can be used during optimization of the baffle design while field simulations are used for final fine-tuning purposes. This helps to minimize the overall engineering and computation effort. Conclusions are given in Section VI.

II. OVERVIEW OF METOP-SG SATELLITES

MetOp-SG space segment will be composed of two Low Earth Orbit (LEO) satellites, called "Satellite A" and "Satellite B". The satellites are housing different payload instruments sensing the Earth, see Figure 1.
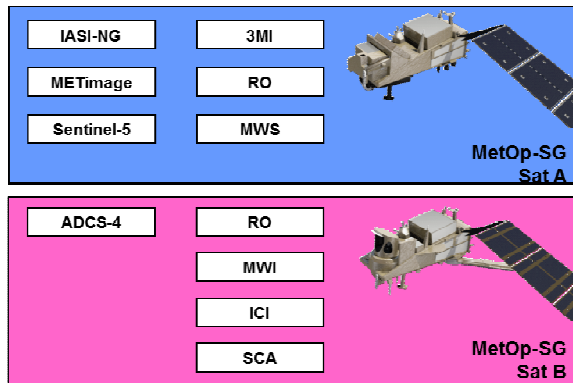

Figure 1.   Allocation of payload instrument on-board the MetOp-SG satellites; left: Customer Furnished Instruments; right: Contractor Furnished Instruments
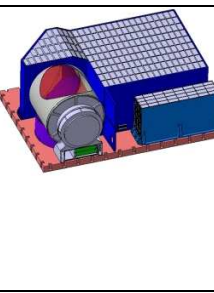
The full names of the instruments are:
- IASI-NG: Infrared Atmospheric Sounding Interferometer - New Generation
- 3MI: Multi-viewing, Multi-channel, Multi-polarisation Imager
- RO: Radio Occultation
- MWS: MicroWave Sounder
- METimage and Sentinel-5: no further name
- A-DCS 4: ARGOS Advanced Data Collection System 4
- MWI: MicroWave Imager
- ICI: Ice Cloud Imager

- SCA: SCAtterometer

Table I shows the geometry and the basic sensing functions of the instruments on-board Satellite A ([3], [4]) based on the status at System Requirements Review (SRR).

TABLE I.   INSTRUMENTS ON-BOARD SATELLITE A

	IASI-NG Atmospheric temperature and humidity profiles; monitor various trace gases (for example ozone [O_3], carbon monoxide [CO], methane [CH_4], carbon dioxide [CO_2]) Frequency range: infrared sensing with wavenumber $k=2\pi/\lambda$ ranging from 645 cm^{-1} to 2760 cm^{-1} and a spectral resolution of 0.25 cm^{-1}.
	METimage High resolution information on clouds, cloud cover, land surface properties, sea, ice and land surface temperatures, etc. Frequency range: Optical imaging with 20 channels between 0.443 μm and 13.345 μm
	Sentinel-5 Ozone and other atmospheric gases profile & column, aerosols optical depth; monitor various trace gases, monitor air quality and support climate monitoring Frequency range: From 0.27 μm (ultraviolet) to 2.385 μm (near infrared)
	3MI Aerosols (optical thickness, particle size, type, height, absorption) , volcanic ashes, surface albedo Frequency range: 12 channels from 0.41 μm to 2.13 μm

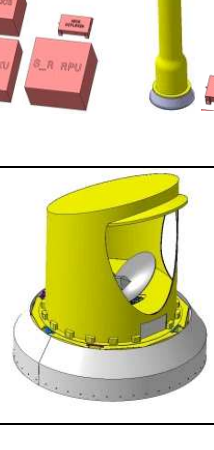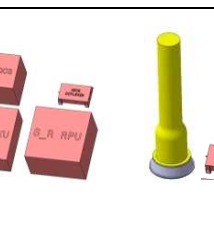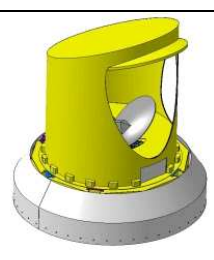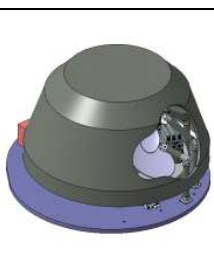|	
	MWS Atmospheric temperature and humidity profiles in clear and cloudy air, cloud liquid water total column Frequency range: RF channels at center frequencies between 23.8 GHz and 189 GHz
	RO Temperature, pressure and humidity profiles, electron contents in ionosphere Frequency range: Band L1: 1.57542 GHz +/- 10.23 MHz Band L5: 1.17645 GHz +/- 10.23 MHz

Table II shows the geometry and the basic sensing functions of the instruments on-board Satellite B ([2], [3]).

TABLE II. INSTRUMENTS ON-BOARD SATELLITE B

	A-DCS 4 Collection of in-situ oceanographic and meteorological data Frequency range: ~ 400 MHz
	MWI Precipitation & cloud products, water vapour profiles & imagery, sea ice Frequency range: RF channels at center frequencies between 18.7 GHz and 191 GHz
	ICI Cloud products (ice clouds), snowfall detection and quantification Frequency range: Different RF channels between 180 GHz and 669 GHz

	SCA (Tx + Rx) Ocean surface wind vectors and soil moisture Frequency range: 5.355 GHz +/- 1 MHz
In addition: RO instrument (see Table 1)	

In addition, both satellites are housing a TT&C system in S-Band (transmitter and receiver) and transmitters in X-Band and Ka-Band for downlink of the sensed data towards Ground.

When the downlink transmitters are active (transmission via Tx antenna), it has to be ensured that the instrument receivers are not distorted by the emissions. Although the on-board Tx antennas are designed to radiate towards the Earth, the field strength around a Tx antenna is not negligible potentially leading to interference seen by the on-board receivers [5]. Limiting this effect is key to proper performance of the receivers. Reduction of unintended interference power can be achieved by, e.g., sufficiently large distances among Tx and Rx antennas, optimization of antenna patterns and inclusion of additional baffles to avoid Line-of-Sight links between Tx and Rx antennas.

For readability reasons, the remaining part of the contribution will use the wording "Transmitter (Tx)" and "Receiver (Rx)" in the sense of the dedicated antennas. Figure 2 shows a preliminary model (at System Requirements Review) of "Satellite A" together with the positions of an exemplary Tx radiating in the X-Band towards the Earth, the Microwave Sounder (MWS) instrument receiver, a baffle and the Nadir direction (towards the Earth during flight).
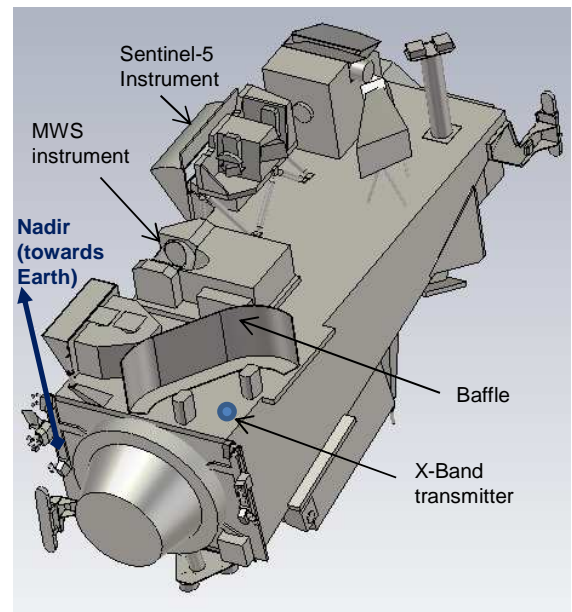

Figure 2. Model of "Satellite A" being part of MetOp Second Generation: Exemplary transmitter and instrument receiver positions

III. FUNDAMENTALS OF RFC ANALYSIS

When multiple transmitters and receivers operating in RF range are located on-board a satellite, potential interference is an issue, and a Radio Frequency Compatibility analysis has to be performed to ensure proper performance. For this purpose, coupling factors between involved Tx and Rx constellations are determined and the resulting interference level at the Rx position is compared to a specified limit.

In the following paragraph, the coupling factor is derived for free space propagation as a function of distance and the angle dependent antenna gain between Tx and Rx. In addition, the analysis takes into consideration

- Improvement of Tx-Rx decoupling for receivers integrating over a pulsed signal (MWI / SCA)
- Additional attenuation in case of No-Line of Sight between Tx and Rx (e.g., shading by structure or intended baffles); hereby, the attenuation value is based on 3D full-wave electro-magnetic simulations (CST Microwave Studio software).

A. Modeling of Interference Power

The approach presented below assumes free space propagation between a Tx and Rx, where the Tx radiates a power P_{Tx} at a frequency f and the victim Rx receives the signal in-band as an interference signal. Figure 3 shows a general constellation involving Tx, Rx, antenna patterns and the definition of elevation angles towards the LoS path.
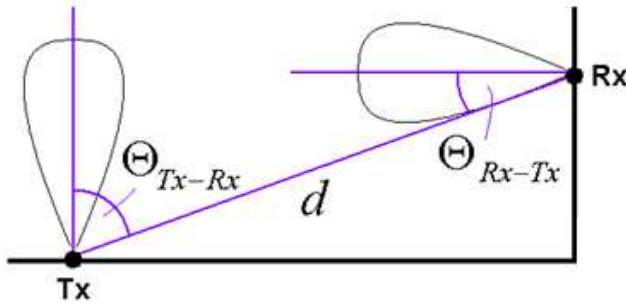

Figure 3. General definition of angles between transmitter and receiver

If the antenna patterns are also dependent on the azimuth angle, azimuth has to be considered as well.

In general, the power density S (in W/m²) at a victim Rx which has been generated by a Tx antenna can be determined as

$$S = \frac{P_{Tx} \cdot G_{Tx}\left(\Theta_{Tx-Rx}, \varphi_{Tx-Rx}\right)}{4\pi \cdot d^2} \tag{1}$$

where P_{Tx} is the total transmitted Power, $G_{Tx}(\Theta_{Tx-Rx}, \varphi_{Tx-Rx})$ is the Tx antenna gain at the considered frequency f in the direction of the Rx (direction described by the elevation

angle Θ_{Tx-Rx} and the azimuth angle φ_{Tx-Rx}), and d is the distance between Tx and Rx.

The Rx antenna will suffer interference from the incident signal. The received interference power P_{Rx} at a distance of d is

$$P_{Rx} = S \cdot A_{eff} = \frac{P_{Tx} \cdot G_{Tx}\left(\Theta_{Tx-Rx}, \varphi_{Tx-Rx}\right)}{4\pi \cdot d^2}$$
$$\cdot \frac{G_{Rx}\left(\Theta_{Rx-Tx}, \varphi_{Rx-Tx}\right) \cdot c_0^2}{4\pi \cdot f^2} \tag{2}$$

where $G_{Rx}(\Theta_{Rx-Tx,}, \varphi_{Rx-Tx})$ is the antenna gain of the victim Rx towards the Tx, f is the Rx frequency, A_{eff} the effective area of the antenna, and c_0 the speed of light in vacuum. This equation describes free space propagation and is known as Friis equation. It assumes that the Rx is positioned in the far field of the transmitter: For antennas physically larger than $\lambda/2$ (where λ is radiated wavelength), the Rx is in the far field of the Tx for $d > d_f = 2D^2/\lambda$ (far field condition). The parameter D corresponds to the physical length of an antenna, or the diameter of a "dish" antenna. In addition, the following conditions have to be fulfilled: $d_f \gg D$ and $d_f \gg \lambda$.

The received power may be attenuated due to harness losses between the Rx antenna and the receiver input (e.g., 2 dB losses). This can be respected by a factor L_{har} ($\leqslant 1$) in the equation. The interference power at the receiver input is then

$$P_{Rx} = L_{har} \cdot \frac{P_{Tx} \cdot G_{Tx}\left(\Theta_{Tx-Rx}, \varphi_{Tx-Rx}\right)}{4\pi \cdot d^2}$$
$$\cdot \frac{G_{Rx}\left(\Theta_{Rx-Tx}, \varphi_{Rx-Tx}\right) \cdot c_0^2}{4\pi \cdot f^2} \tag{3}$$

The coupling factor is defined as the ratio between the received and the transmitted power. Above equation leads to

$$C = \frac{P_{Rx}}{P_{Tx}}$$
$$= L_{har} \cdot G_{Tx}\left(\Theta_{Tx-Rx}, \varphi_{Tx-Rx}\right) \tag{4}$$
$$\cdot \frac{G_{Rx}\left(\Theta_{Rx-Tx}, \varphi_{Rx-Tx}\right) \cdot c_0^2}{\left(4\pi \cdot d \cdot f\right)^2}.$$

Hereby, the expression $c_0^2 / (4 \pi d f)^2$ is also called free space loss. The coupling factor is hence the free space loss multiplied by the loss factor L_{har} at Rx side and the antenna gain of both Tx and Rx antenna in the LoS direction.

The coupling factor in dB is obtained by applying "10*log$_{10}$" of the linear value. In satellite design with distances in the range of meters and frequencies in RF range, a typical coupling factor is, e.g., -100 dB.

The sensitivity of the victim receiver describes the maximal allowed interference power (e.g., value in mW or dBm in logarithmic notation) at Rx side. The interference power P_{Rx} shall be smaller than the specified sensitivity, where the difference is called RFC margin. An RFC margin of 20 dB is typically recommended in an early project phase. Sometimes, the sensitivity of the receiver is not given in terms of power, but in terms of power spectral density (=PSD, e.g., in mW/Hz or dBm/Hz in logarithmic notation). In this case, power has to be replaced by PSD values in above equations. This leads to

$$PSD_{Rx} = L_{har} \cdot \frac{PSD_{Tx} \cdot G_{Tx}\left(\Theta_{Tx-Rx}, \varphi_{Tx-Rx}\right)}{4\pi \cdot d^2} \cdot \frac{G_{Rx}\left(\Theta_{Rx-Tx}, \varphi_{Rx-Tx}\right) \cdot c_0^{\ 2}}{4\pi \cdot f^2} \qquad (5)$$

where PSD_{Tx} is the power spectral density of the Tx signal at frequency f and PSD_{Rx} is the power spectral density of the Rx signal at frequency f. In this case, the coupling factor is defined as

$$C = \frac{PSD_{Rx}}{PSD_{Tx}} = L_{har} \cdot G_{Tx}\left(\Theta_{Tx-Rx}, \varphi_{Tx-Rx}\right) \cdot \frac{G_{Rx}\left(\Theta_{Rx-Tx}, \phi_{Rx-Tx}\right) \cdot c_0^{\ 2}}{\left(4\pi \cdot d \cdot f\right)^2}. \qquad (6)$$

The resulting coupling factor is hence the same when compared to the previous definition, which was based on power. The interfering power spectral density PSD_{Rx} shall be smaller than the specified sensitivity, where the difference is called RFC margin. If the LoS is shaded, e.g., by a dedicated baffle, an additional loss factor has to be considered in above equation. In this case, the coupling factor can be described by:

$$C = L_{har} \cdot L_{baffle} \cdot G_{Tx}\left(\Theta_{Tx-Rx}, \varphi_{Tx-Rx}\right) \cdot \frac{G_{Rx}\left(\Theta_{Rx-Tx}, \varphi_{Rx-Tx}\right) \cdot c_0^{\ 2}}{\left(4\pi \cdot d \cdot f\right)^2}. \qquad (7)$$

Above considerations are based on in-band interference. In general, this case can be avoided by proper selection of Tx and Rx frequencies. Nevertheless, interference may occur, e.g., since the Tx radiates, in addition to the desired signal.

- Out-of-band noise: This means that the Tx radiates noise power outside the desired Tx frequency range. The coupling factor is determined in the same way as for in-band considerations.
- Out-of-band spurious (harmonics): Hereby, the Tx radiates also an integer multiples of the carrier frequency f_c. The n-th harmonic is associated with a frequency of $n*f_c$. The coupling factor between the n-th harmonic and the Rx is calculated by the same equation as shown above, but f has to be replaced by $n*f_c$.

As a rule of thumb, if no sensitivity value is specified, the received interference power should be about 20 dB below the minimal input level of the receiver which may be, e.g., -120 dBm. In reality, a victim Rx may receive multiple interference signals simultaneously that originate, e.g., from different transmitters. In this case, the sum of all contributions at the considered frequency must still provide sufficient RFC margin (e.g., 20 dB).

B. Methods to Achieve Strong Decoupling

Equation (7) indicates that strong decoupling between a Tx and a Rx can be achieved by a high baffle attenuation, sufficiently low antenna gain at both Tx side and Rx side in LoS direction, large distance, low Tx power and high Tx frequency. In case of harmonics radiation, the radiated power of the harmonic signal can, e.g., be minimized by proper RF filtering.

C. Temporal Effects

On MetOp-SG "Satellite B", the Scatterometer (SCA) radiates pulsed signals. For combinations with SCA Tx and MWI Rx, the pulsed nature of SCA signals leads to an improvement of the decoupling between Tx and Rx, as described hereafter.

The SCA (only present on Satellite B) radiates a pulsed signal. This means that the signal (and hence the power spectral density in dBm/Hz) is only present during the pulse duration T_P. The MWI receiver hence observes a power spectral density of $S(t)=S_0$ during T_P, else zero. The MWI instrument integrates $S(t)$ over the integration time $T_{int} > T_P$ which leads to

$$\int_0^{T_{int}} S(t)dt = S_0 \cdot T_P = S_{0,red} \cdot T_{int} \qquad (8)$$

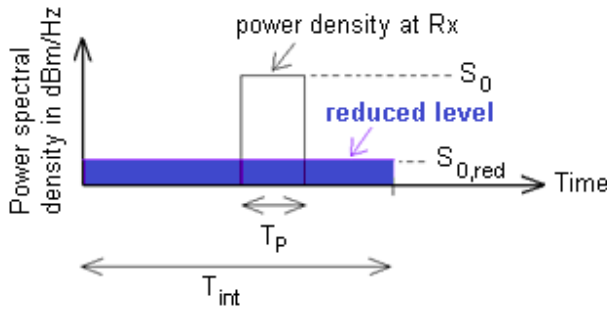where $S_{0,red}$ is the effective reduced power spectral density as indicated in Figure 4.

Figure 4. Temporal effects on power spectral density

This means:

$$S_{0,\text{red}} = S_0 \cdot \frac{T_\text{P}}{T_\text{int}}. \tag{9}$$

In logarithmic notation, the received power spectral density is hence $S_{0,\text{red}}[\text{dBm/Hz}] = S_0[\text{dBm/Hz}] + 10*\log (T_\text{P}/T_\text{int})$ whereas the second term provides a negative value (hence $S_{0,\text{red}}$ is lower than S_0). $|10*\log (T_\text{P}/T_\text{int})|$ describes the improvement of the decoupling between Tx and Rx due to temporal effects, which translates into a respective improvement of the RFC margin.

IV. APPROACH TO DETERMINE BAFFLE INFLUENCE

This section assumes a metallic baffle (e.g., wall) between a Tx and a victim Rx to limit undesired signals at the Rx position. The physics of electromagnetic wave propagation at radio frequencies is the reason for an undesired signal still present at the Rx position, albeit strongly attenuated: Signal paths originating from diffraction at the baffle can travel towards the Rx as a result of Huygen's principle. In addition, further signal contributions may originate from reflections or scattering at objects in the vicinity of the Tx and Rx. The principle of this multipath propagation is visualized in Figure 5. Hereby, the shown diffracted path interacts with the baffle directly above the hypothetical LoS path. In general, further diffracted paths are possible with interaction points along the top of the baffle.
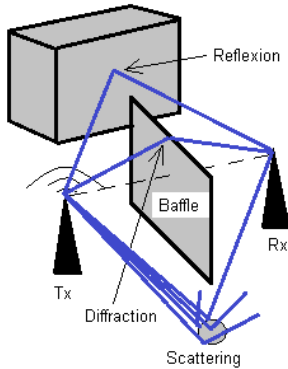

Figure 5. Multipath propagation

Since reflected and scattered paths can carry significant power levels, these contributions should be avoided by a proper design of the baffle (e.g., by an adequate height and an adequate length around the surrounding objects). In this case, the dominant contribution at Rx side only results from the diffraction at the baffle. Due to the physics of diffraction, the interfering signal decreases with steeper diffraction angle (e.g., increased baffle height) and frequency.

The influence of a baffle on the received signal can be determined either by:

- A simplified wave propagation model, e.g., theory of knife-edge diffraction.
- 3D field simulations: A simulation tool solves the corresponding electromagnetic field equations and determines the received field strength at the Rx. This method implicitly takes into account diffraction, reflection and scattering.

A. Analytical Approach by Knife-edge Diffraction

The scenario related to "knife-edge diffraction" is visualized in Figure 6. It assumes a "knife-edge" obstacle between Tx and Rx and shows the diffracted path between Tx and Rx. Hereby, the obstacle subdivides the distance between Tx and Rx into d_1 and d_2. Two cases are possible: In case 1, the upper edge of the obstacle appears at a height $h > 0$ w.r.t. the Line of Sight (LoS). This leads to a "No Line of Sight" (NLoS) scenario. In case 2, the upper edge of the obstacle appears at a height $h < 0$ w.r.t. LoS. This leads to a LoS scenario.
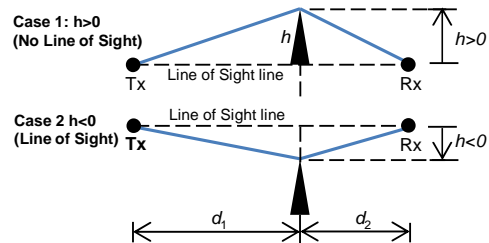

Figure 6. Diffraction at a "knife-edge" for two cases: "No Line of Sight" and "Line of Sight"

According to [6] and [9], the loss induced by the baffle (diffraction loss) is

$$L_{dB} = -20 \cdot \log_{10} |F(v)| \tag{10}$$

with the complex Fresnel integral

$$F(v) = \frac{1+j}{2} \cdot \int_v^\infty e^{-j\pi t^2/2} dt \tag{11}$$

and

$$v = h \cdot \sqrt{\frac{2}{\lambda} \cdot \left(\frac{1}{d_1} + \frac{1}{d_2} \right)} \tag{12}$$

where v is the Fresnel-Kirchhoff diffraction parameter and $\lambda = c_0/f$ is the wavelength of the considered signal. The

resulting diffraction loss ("baffle attenuation") as a function of v is plotted in Figure 7 for $v = [-5 .. 5]$ as per [7].

Figure 7. Diffraction loss of a "knife-edge" versus parameter v [7]

The figure shows the level of the diffracted path in dB relative to freespace, which is negative for $v > -0.7$. Hereby, a level of "$-x$ dB" corresponds to an attenuation of "x dB". According to (12), v and h are proportional, hence, $h > 0$ (NLoS) is associated with $v > 0$, yielding a baffle attenuation of at least 6 dB (see graph). The above graph can be approximated, e.g., by the following piecewise function [8]:

$$L_{dB} = \begin{cases} -(6 + 9 \cdot v - 1.27v^2) & \text{if } 0 \le v \le 2.4 \\ -(13 + 20 \cdot \log_{10}(v)) & \text{if } v > 2.4 \end{cases} \quad (13)$$

Note that above equation is the good one compared to a sign error related to $1.27v^2$ in [8]. To quickly determine the "baffle attenuation", the approach is to determine v by (12) and then to apply (13) for the obtained v.

Example (typical values on a satellite): For $d_1 = 1.5$ m, $d_2 = 1.5$ m and $f = 8.2$ GHz (X-Band as typical downlink case), Figure 8 visualizes the "baffle attenuation" as a function of the parameter h.
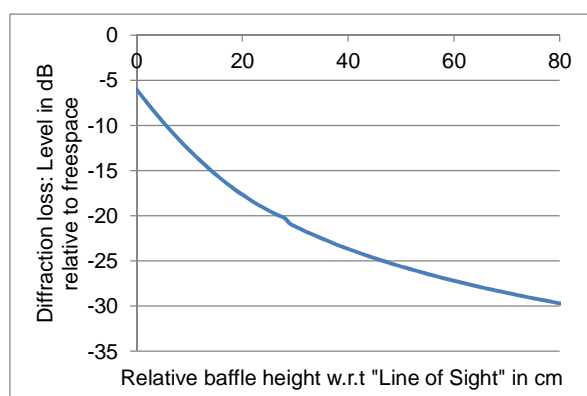

Figure 8. Diffraction loss of a "knife-edge" versus h assuming $d_1 = 1.5$ m, $d_2 = 1.5$ m and $f = 8.2$ GHz

The result reveals that the attenuation is very sensitive to the height. This behavior is due to the small wavelength which is only 3.7 cm in the considered case.

The other way around, the theory of knife-edge diffraction reveals that the baffle attenuation in X-Band frequency range can be improved significantly by only slightly increasing the baffle height. In practice, constraints on the height are given by the required field of views of the transmitters and instruments.

B. Simulation based approach (CST field simulation)

An approach based on solving electromagnetic field equations has the following advantages:

- Result available for any baffle geometry (not only for simple objects like a "knife-edge")
- All wave propagation phenomena implicitly taken into account (e.g., also reflection and scattering), not only diffraction as in the "knife-edge model"
- Environment (surrounding structure) can be taken into account

A well suited approach for satellite engineering is to use the simulation software "Microwave Studio" from the company CST. For example, this tool has also been used by Airbus Defence and Space to assess EMC/RFC for MTG satellites.

To determine the baffle attenuation, a dipole antenna is placed at the transmitter position and oriented in a way that the radiation towards the receiver position is maximized. The electric field strength in dB(mV/m) at a victim receiver is first simulated without baffle (reference, including Line of Sight path) and then with baffle. In both cases, the surrounding satellite structure is taken into account. The difference of the electric field strength in dB(mV/m) corresponds to the baffle attenuation in dB.

To obtain the simulation results reported in this paper, the integral equal solver based on Multi Level Fast Multipole Method (MLFMM) has been used. MLFMM is a technique based on the same principles as the traditional "Method of Moments" (MoM), but applicable to models of significantly larger electrical size. Given the geometrical dimensions of typical Earth observation satellites, simulations at frequencies as high as (roughly) 30 GHz can be performed applying this numerical technique. Higher frequencies (smaller wavelengths) require a mesh size that results in increased memory demand and simulation time. Should the need arise to overcome that constraint for practical limitations (e.g., memory size), the satellite structure can be restricted to a representative volume encompassing the Tx and Rx positions.

V.   COMPARISON OF FIELD SIMULATIONS W.R.T. KNIFE-EDGE THEORY

On Satellite A, the radiation of the X-Band transmitter towards the MWS instrument is reduced by a baffle (height:

65cm). Figure 9 visualizes a part of the satellite structure including the phase center of the transmitter (modeled as a dipole) radiating at 8.2 GHz, the baffle as well as the MWS victim receiver. Hereby, two Rx positions ("Position 1", "Position 2") are considered, where "Position 2" corresponds to the center of the MWS reflector plate. The figure also shows the position of the Sentinel-5 instrument.
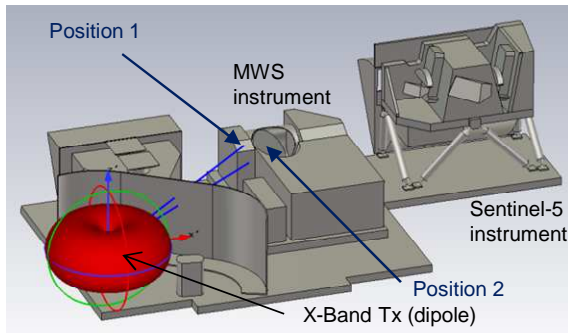

Figure 9.   Part of the structure of Satellite A (dipole Tx)

The figure also indicates the LoS directions between Tx and the two Rx positions. The electric field strengths are simulated with the CST software for two scenarios:

- "without baffle"
- "with baffle".

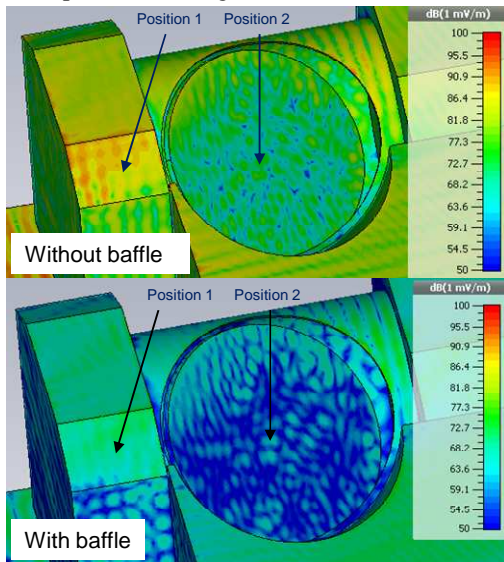Results are presented in Figure 10.

Figure 10. Simulated field strength at MWS assuming radiating dipole; f=8.2 GHz

Observation:
Position 1: The case "Without baffle" reveals a field strength of 90 $\pm$ 1 dBmV/m". The case "With baffle" reveals 72 $\pm$ 1 dBmV/m. Hence, the difference is 18 dB.

Position 2: The case "Without baffle" reveals a field strength of $\approx$ 77 dBmV/m". The case "With baffle" reveals $\approx$ 64 dBmV/m. Hence, the difference is 13 dB.

In a second step, the attenuation is estimated by applying the theory of knife-edge diffraction. As explained in the section on knife-edge theory, the baffle subdivides the theoretical LoS path into two distances (d_1, d_2) and a relative height h of the baffle. For "Position 1", the values are: $d_1 =$ 1.07 m, $d_2 = 1.08$ m, $h = 0.16$ m. Assessment at $f = 8.2$ GHz yields an expected baffle attenuation of 17.2 dB while 18 dB has been simulated by CST software according to the previous figure. This shows a good agreement between simplified theory and CST simulations. Assessment for "Position 2" ($d_1 = 1.05$ m, $d_2 = 1.43$ m, $h = 0.218$ m) at $f =$ 8.2 GHz yields an expected baffle attenuation of 18 dB while 13 dB has been simulated by CST software. This behavior can be explained as follows: In contrast to "Position 1", "Position 2" does not enable a path directly diffracted at the baffle towards the receiver position. The signal can arrive at "Position 2" only via multiple interactions, hence, the knife-edge diffraction theory based on a single baffle is not applicable.

Next, the radiation pattern of the Tx antenna is replaced by the measured characteristics of the physical X-Band helix antenna. Figure 11 visualizes the 3D pattern as well as the antenna gain as a function of elevation angle Θ.
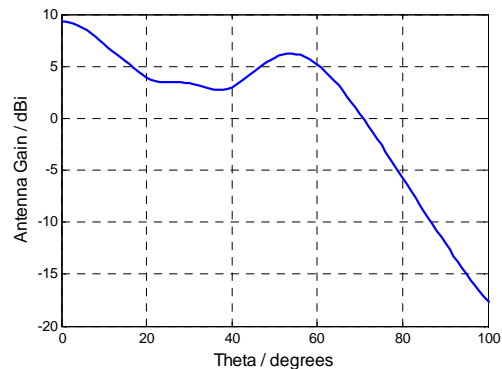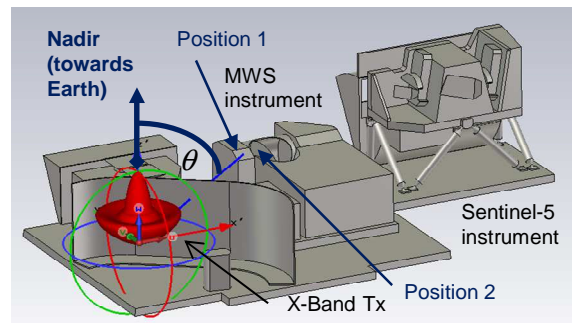

Figure 11. Scenario with real antenna pattern; antenna performance

For the analysis, "Position 1" is considered. The CST simulation as per Figure 12 reveals: The case "Without baffle" leads to a field strength of 80.8 $\pm$ 1

dBmV/m" while "With baffle" leads to 70.8 ± 1 dBmV/m. Hence, the difference caused by the baffle is 10 dB.
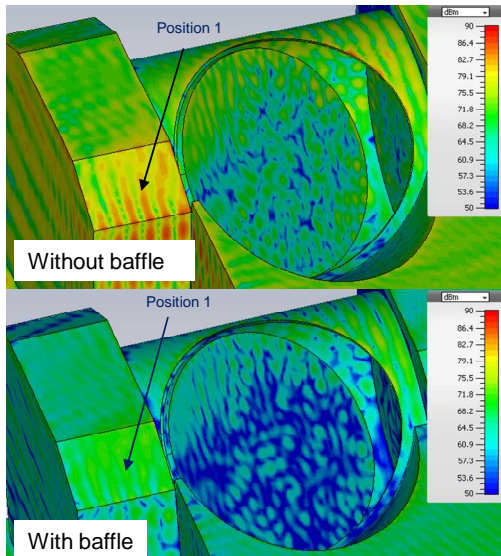

Figure 12. Simulated field strength at MWS assuming real antenna pattern; *f*=8.2 GHz

The question arises if this value of 10 dB attenuation can be predicted by the knife-edge diffraction theory. To do so, the angle-dependent antenna data has been incorporated into the knife-edge diffraction theory. The approach is described hereafter: First, the elevation angle is determined under which a propagation path leaves the transmitter. Figure 13 shows the principal scenario.
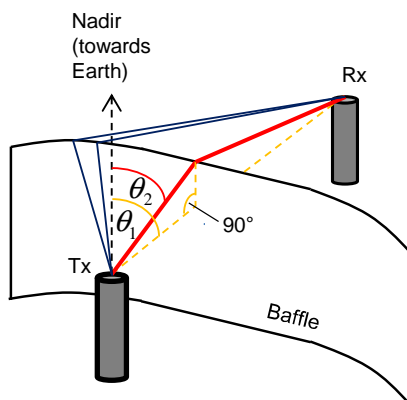

Figure 13. Principal scenario involving diffracted paths

- A dotted line indicates the propagation path in LoS direction which is present in absence of the baffle. The associated elevation angle is Θ_1.

- In presence of a baffle, a path originating from diffraction appears at an angle $\Theta_2 < \Theta_1$. Hereby, the interaction point with the baffle is inside the plane defined by the Nadir direction and the LoS direction.

For "Position 1", the elevation angles and the associated antenna gain according to Figure 11 are:
- $\Theta_1 = 89.9$ deg, associated with a gain of -12.5 dBi.
- $\Theta_2 = 82.4$ deg, associated with a gain of -7.3 dBi.

Hence, the diffracted path runs along a direction with higher gain when compared to the LoS direction. Therefore, it is expected that the influence of the baffle is lower compared to the dipole case. The expected attenuation by insertion of the baffle corresponds to the result of the dipole, corrected by the delta antenna gain, hence, the expected value is 17.2 dB – ((-7.3) - (-12.5)) dB = 12 dB.

For comparison, 10 dB attenuation has been determined using the CST simulation software. Limited differences in the result can be explained, e.g., by

- Multipath propagation:
  While above consideration assumes only one diffracted path, further diffracted paths are possible along the top of the baffle. These additional paths occur out of the plane which is defined by Nadir direction and LoS direction. Possible additional paths are already visualized in the left part of Figure 13. In principle, all paths have to be weighted by the angle-dependent antenna gain and then summed up. As the knife-edge theory does not predict multiple paths and the associated elevation angles, only weighting of the diffracted path "in-plane" is possible. A more complex channel model which predicts multiple paths and allows for insertion of an angle dependent antenna gain is Ray-tracing [10]. A disadvantage of this technique is however increased computational time.
- Baffle geometry:
  The baffle geometry differs from the ideal "knife-edge theory" as the baffle is bended and the distance between Tx and baffle differs along the baffle.
- Approximation of Fresnel integral :
  Equation (13) is only an approximation of (10).

To verify the effect of baffles on-board the MetOp-SG satellites prior to launch, measurements are envisaged in the frame of ground testing. These so-called mock-up tests will be performed in Q2/2016 and use transmitters and receivers with representative antenna pattern as well as a relevant part of the satellite structure.

A similar approach using an adapted knife-edge model is shown in [11], which considers the channel between a train and a satellite including a knife-edge obstacle that models structural elements on the roof of the train. In [11], classical knife-edge theory is expanded by only one antenna gain (the "train antenna gain"), whereas the present contribution takes into account both the characteristics of the transmitter and the receiver.

Finally, a general remark is given w.r.t. field predictions when involving antenna patterns: The radiation pattern of a transmit antenna differs between the near-field and the far field where far field conditions are achieved at distances of $d > d_{\min} = 2\,D^2\,/\,\lambda$ (D = antenna dimension). When using a far field antenna pattern in above approach, the distance between the transmit antenna and the baffle has to be at least $d_{\min}$ (fulfilled in above consideration). A near field approach considers possible pattern distortion by the baffle.

VI. Conclusions

Modern Earth observation satellites such as the MetOp-SG satellites accommodate manifold Radio Frequency transmitters and instrument receivers. The on-board transmitters generate an electromagnetic environment with potential impact on the performance of instrument receivers. Ensuring Radio Frequency Compatibility means that the level of the unintended signal at Rx side is kept below a certain threshold level so that the instrument performance is not degraded. The satellite configuration (for example, position and orientation of on-board transmitters and receivers) is vital to RFC. As a consequence, it deserves careful consideration throughout the satellite program, starting with a first optimization in a very early project phase.

The suitability of the configuration w.r.t. RFC is verified by an RFC analysis, which is based on the calculation of the coupling factor between critical combinations of Tx and Rx. An RFC analysis covers both in-band-radiation and out-of-band radiation (e.g., radiation of wideband noise or harmonics). A correction factor leading to improved decoupling should be applied when a pulsed signal is received by a receiver applying integration times in excess to the pulse width of the interfering signal. In case of insufficient decoupling between Tx and Rx, the situation can be improved by a dedicated baffle between Tx and Rx, optimization of antenna orientations, increased distance, lower Tx power or stronger filtering effort at Tx side.

Conclusions related to a proper design of a baffle are given hereafter: The height of the baffle shall be large enough to
- realize NLoS between Tx and Rx (and hence, a diffracted path towards the Rx)
- avoid reflections at, e.g., high objects in the vicinity of Tx and Rx

The length of the baffle shall be large enough to avoid reflections at objects next to the baffle which could carry significant power towards the Rx.

To determine the baffle attenuation for such a properly designed baffle, two methods have been studied: 3D field simulations and knife-edge diffraction theory (based on a single baffle), expanded by information on antenna gain. It has been shown that the results agree well in scenarios resembling the set-up illustrated in Figure 13, involving a single diffraction of the wave propagating from Tx to Rx. Hence, the simplified theory is an adequate method for assessing the effectiveness of the baffle prior to initiating extensive 3D full-wave simulations. This approach minimizes the overall engineering and computation effort. Verification of the derived results for MetOp-SG will be achieved by mock-up testing in Q2/2016.

References

[1] J. Timmermann, C. Imhof, D. Lebherz, and J. Lange, "Application of Knife-Edge Diffraction Theory to Optimize Radio Frequency Compatibility On-board a Satellite," The Seventh International Conference on Advances in Satellite and Space Communications (SPACOMM), April 2015, ISBN: 978-1-61208-397-1, pp. 7-12.

[2] Statement Of Work for MetOp Second Generation (MetOp-SG) Phase B2/C/D/E, ESA UNCLASSIFIED – For Official Use, MOS-SOW-ESA-SYS-0494, issue 1, 09/09/2013.

[3] MetOp Second Generation (MetOp-SG) Space Segment Requirements Document (SSRD), MOS-RS-ESA-SYS-0001, 09/09/2013

[4] Monitoring Weather and Climate from Space – EPS-SG Overview for CSPP / IMAPP User's Group Meeting, 15 April 2015; http://www.ssec.wisc.edu/meetings/cspp/2015/Agenda%20PDF/Wednesday/Schluessel_EPS-SG_CSPP_IMAPP.pdf

[5] J.A. Miller and A.R. Horne, "Radio frequency compatibility design and testing on the polar platform spacecraft," Electromagnetic Compatibility, 10th International Conference on Electromagnetic Compatibility (Conf. Publ. No. 445), pp. 35-40, 1-3 Sept. 1997

[6] K. Du and M. Swamy, Wireless Communication Systems: From RF Subsystems to 4G Enabling Technologies. Cambridge University Press, 2010.

[7] http://www.mike-willis.com/Tutorial/PF7.htm [retrieved: Feb., 2015]

[8] www.wirelesscommunication.nl/reference/chaptr03/diffrac.htm [retrieved: Feb., 2015]

[9] C. Hasslet, Essentials of Radio Wave Propagation. Cambridge Wireless Essentials Series, Cambridge University Press, 2008.

[10] J. Timmermann, M. Porebska, C. Sturm, and W. Wiesbeck, "Investigating the Influence of the Antennas on UWB System Impulse Response in Indoor Environments," 37th European Microwave Week (EuMW), Oct. 2007, pp. 1562-1565.

[11] S. Scalise, H. Ernst, and G. Harles. "Measurements and modeling of the land mobile satellite channel at Ku-Band," IEEE Transactions on Vehicular Technology, 57 (2), pp. 693-703, March 2008.